Chemical Geology 525 (2019) 18–27

Contents lists available at ScienceDirect

Chemical Geology

journal homepage: www.elsevier.com/locate/chemgeo

Mechanisms of olivine dissolution by rock-inhabiting fungi explored using magnesium stable isotopes

Rasesh Pokharel[a,b,*], Ruben Gerrits[c,d], Jan A. Schuessler[a,1], Friedhelm von Blanckenburg[a,b]

[a] GFZ German Research Centre for Geosciences, Section 3.3, Earth Surface Geochemistry, Telegrafenberg, 14473 Potsdam, Germany
[b] Institute of Geological Sciences, Freie Universität Berlin, 12249 Berlin, Germany
[c] BAM Federal Institute for Materials Research & Testing, Department 4, Materials & Environment, 12205 Berlin, Germany
[d] Department of Biology, Chemistry and Pharmacy, Freie Universität Berlin, 14195 Berlin, Germany

ARTICLE INFO

Editor: Michael E. Boettcher

Keywords:
Weathering
Mineral Dissolution
Olivine
Metal Stable Isotopes
Microbiology

ABSTRACT

To unravel the dissolution mechanisms of olivine by a rock-inhabiting fungus we determined the stable isotope ratios of Mg on solutions released in a laboratory experiment. We found that in the presence of the fungus *Knufia petricola* the olivine dissolution rates were about seven-fold higher (1.04×10^{-15} mol cm^{-2} s^{-1}) than those in the abiotic experiments (1.43×10^{-16} mol cm^{-2} s^{-1}) conducted under the same experimental condition (pH 6, 25 °C, 94 days). Measured element concentrations and Mg isotope ratios in the supernatant solutions in both the biotic and the abiotic experiment followed a dissolution trend in the initial phase of the experiment, characterized by non-stoichiometric release of Mg and Si and preferential release of ^{24}Mg over ^{26}Mg. In a later phase, the data indicates stoichiometric release of Mg and Si, as well as isotopically congruent Mg release. We attribute the initial non-stoichiometric phase to the rapid replacement of Mg^{2+} in the olivine with H^+ along with simultaneous polymerization of Si tetrahedra, resulting in high dissolution rates, and the stoichiometric phase to be influenced by the accumulation of a Si-rich amorphous layer that slowed olivine dissolution. We attribute the accelerated dissolution of olivine during the biotic experiment to physical attachment of *K. petricola* to the Si-rich amorphous layer of olivine which potentially results in its direct exposure to protons released by the fungal cells. These additional protons can diffuse through the Si-rich amorphous layer into the crystalline olivine. Our results also indicate the ability of *K. petricola* to dissolve Fe precipitates in the Si-rich amorphous layer either by protonation, or by Fe(III) chelation with siderophores. Such dissolution of Fe precipitates increases the porosity of the Si-rich amorphous layer and hence enhances olivine dissolution. The acceleration of mineral dissolution in the presence of a rock-dissolving fungus further suggests that its presence in surficial CO_2 sequestration plants may aid to accelerate CO_2 binding.

1. Introduction

Fungi are ubiquitous in the terrestrial environment and can live in soils and rocks, or be in symbiosis with plant roots or other microbes (Burford et al., 2003a; Burford et al., 2003b; Harley and Smith, 1983; Hawksworth, 1988; Warcup, 1951). Several studies confirm the ability of fungi to increase silicate mineral dissolution rates (Banfield et al., 1999; Bonneville et al., 2009; Ehrlich, 1996; Gadd, 2007; Hagerberg et al., 2003; Henderson and Duff, 1963; Rosling et al., 2004). For example, laboratory studies by Balogh-Brunstad et al. (2008) and Bonneville et al. (2011) showed that an ectomycorrhizal (ECM) fungus accelerated biotite dissolution by direct (e.g. tunneling into the mineral and excreting protons and ligands in the contact zone) and indirect (e.g. lowering the pH of the solution by exuding organic acids and by producing CO_2 via respiration) mechanisms. Another study on dissolution of lizardite by the fungus *Talaromyces flavus* in lab experiments concluded that biogenic dissolution accounted for about 40% - 50% of total weathering at steady-state conditions (Li et al., 2016). A contrasting observation by Oelkers et al. (2015) showed that the preferential growth of fungi and bacteria on the surface of Mg silicate minerals potentially slows dissolution rates. These observations call for the role of fungi to be elucidated and quantified in field studies of silicate weathering.

However, in bio-weathering systems a major challenge lies in the need to separate the effects of biotic from abiotic processes that often occur simultaneously. Application of metal stable isotopes can help to

* Corresponding author at: Université de Rennes, Ecole Nationale Supérieure de Chimie de Rennes, CNRS ISCR UMR6226, F-35000 Rennes, France.
E-mail address: rasesh.pokharel@ensc-rennes.fr (R. Pokharel).
[1] Current address: Thermo Fisher Scientific, 28,199 Bremen, Germany.

https://doi.org/10.1016/j.chemgeo.2019.07.001
Received 18 October 2018; Received in revised form 26 June 2019; Accepted 1 July 2019
Available online 04 July 2019
0009-2541/

tackle this challenge. For example, Mg isotopes fractionate during both abiotic (mineral dissolution, secondary mineral formation, carbonate precipitation and ion exchange) (Fries et al., 2019; Maher et al., 2016; Opfergelt et al., 2014; Pearce et al., 2012; Ryu et al., 2016; Schott et al., 2016; Wimpenny et al., 2014; Wimpenny et al., 2010) and biotic (uptake and translocation by microbes and higher plants) processes (Balland-Bolou-Bi et al., 2019; Black et al., 2008; Bolou-Bi et al., 2010; Bolou-Bi et al., 2012; Fahad et al., 2016; Kimmig et al., 2018; Mavromatis et al., 2014; Moynier and Fujii, 2017; Pokharel et al., 2017; Pokharel et al., 2018; Ra and Kitagawa, 2007; Ra et al., 2010; Schmitt et al., 2012; Shirokova et al., 2013; Tipper et al., 2010; Uhlig et al., 2017). In an abiotic dissolution experiment of olivine at pH 2–3 by Wimpenny et al. (2010) showed the preferential release of lighter ^{24}Mg, where after 3 days the dissolved phase was −0.36‰ lower in $^{26}Mg/^{24}Mg$ than the original olivine. An opposite trend was observed by Oelkers et al. (2015) during olivine dissolution in presence of microbes at neutral pH, where the dissolved phase was enriched in the ^{26}Mg, such that after 5 years the solution was 0.25‰ higher in $^{26}Mg/^{24}Mg$ than the dissolving olivine. Maher et al. (2016) interpreted Mg isotope fractionation during experimental forsterite dissolution with a surface kinetic model. During the early stages of olivine dissolution the enrichment of the solution in ^{24}Mg, where its $^{26}Mg/^{24}Mg$ ratio was −0.36‰ lower in than that of the original olivine, was attributed to a surface kinetic effect. At a later stage, a phase called steady state dissolution, the bulk solution attained the isotopic composition of the original olivine. Several studies indicate that Mg isotopes are fractionated during uptake by fungi. A study by Fahad et al. (2016) showed ectomycorrhizal fungus incorporate lighter Mg isotopes from the growth solution where the fungus was about −0.15‰ lower in $^{26}Mg/^{24}Mg$ than the growth solution, whereas a non-mycorrhizal fungus preferentially incorporated heavier Mg isotopes and its Mg was enriched about 0.3‰ in its $^{26}Mg/^{24}Mg$ ratio. A study by Pokharel et al. (2017) showed that rock-inhabiting black fungus *Knufia petricola* preferentially incorporate heavier Mg isotopes during growth and observed a pH-dependence on Mg isotope fractionation: $^{26}Mg/^{24}Mg$ in the fungus was 0.65‰ and 1.11‰ higher in than the growth solution at pH 6 and pH 3 respectively. Given these previous results, we expect that during mineral dissolution Mg isotopes in the solutions track either of the following processes: 1) uptake of Mg into organisms, provided a significant fraction of the Mg released is incorporated into their biomass; 2) the kinetics of mineral dissolution, provided that the fraction of Mg transferred into and remaining in organisms is low.

Here we apply stable isotopes of Mg to a laboratory microcosm batch experiments comprised of the rock-inhabiting microcolonial fungus *Knufia petricola* A95 and the mineral olivine to investigate biogenic mineral dissolution. We chose *K. petricola* as it is commonly found in sub-aerial environments, has the ability to dissolve rocks (Seiffert et al., 2016). The main objectives of this study are to: 1) quantify fungal olivine dissolution rates, and 2) explore the mechanism of biogenic olivine dissolution. We show that in the presence of *K. petricola* dissolution rates increases seven-fold over the abiotic control, and discuss mechanisms that can lead to this acceleration.

2. Materials and methods

2.1. Components of batch experiments

Olivine, $(Mg,Fe)_2SiO_4$, is an orthosilicate, with $[SiO_4]^{4-}$ tetrahedra. Forsterite is its Mg-rich endmember, whereas fayalite is the Fe(II)-rich endmember of the solid-solution series (Kolesov and Geiger, 2004). During weathering of olivine only one ionic Mg-O-bond is broken, and unlike in other silicate minerals, no Si-O-Si bond is broken. Due to this feature olivine is one of the fastest dissolving silicate minerals (Oelkers et al., 2018b), making it well-suited for mineral dissolution studies. The natural olivine mineral used in this study was from San Carlos, Arizona. The olivine mineral grains of ~0.5 cm in size were ground with an agate mortar and pestle and a size fraction of 63 to 125 µm was separated by sieving. This fraction was ultrasonically cleaned multiple times with acetone and deionized water (Merck Millipore) to remove fine particles and then dried at 65 °C for 24 h. The surface area of the cleaned olivine was measured at the Bundesanstalt für Materialforschung und -prüfung (BAM) in Berlin, Germany, by the BET (ASAP 2020, Micromeritics, USA) using the Krypton adsorption method and was 1470 ± 260 (2SD) $cm^2\,g^{-1}$. The chemical composition measured by electron microprobe (JXA 8200, JEOL, USA) at Freie *Universität Berlin* indicates that the average composition of the olivine was $Mg_{1.86(\pm 0.04)}Fe_{0.19(\pm 0.02)}Si_{1(\pm 0.02)}O_4$ (2SD).

The growth media (prepared in bulk volume of 5 l) comprised 0.3 mM Na_2SO_4, 0.173 mM K_2HPO_4, 9.95 µM thiamine hydrochloride, and 18.5 mM NH_4NO_3. The media was autoclaved prior to addition of filter-sterilized glucose as a carbon source (9.96 mM final concentration). Finally 2-(*N*-morpholino) ethanesulfonic acid (MES) (11.1 mM final concentration) was added as a pH buffer.

The fungus used in this study was a relatively fast growing rock-inhabiting microcolonial fungus *Knufia petricola* A95 (formerly known as *Sarcinomyces petricola*). This species is ubiquitous in the terrestrial environment and its geographic distribution ranges from the Mediterranean to the Artic (Gorbushina et al., 2008; Wollenzien et al., 1997). This particular strain was isolated from weathered marble monument in Athens, Greece. The DNA sequence of this fungus has been well-studied (Nai et al., 2013). This species is both biologically relevant due to its ability to form symbiosis with cyanobacteria and geologically important due to its mineral weathering ability (Gorbushina et al., 2008; Seiffert et al., 2016). A detailed description of the cultivation of the strain is given in Nai et al. (2013) and Noack-Schönmann et al. (2014). Prior to cultivation in the batch experiment setup, the fungal biomass strain was washed with EDTA and then the batch supernatant media to remove surficial contamination.

2.2. Dissolution experiment

All dissolution experiments were done as batch experiments. Four grams of ground olivine powder were distributed over six pre-cleaned 500 ml polycarbonate Erlenmeyer flasks with vented caps which were then autoclaved for microbial sterilization. 400 ml of growth media was placed in each of the Erlenmeyer flask. In each of three Erlenmeyer flasks, 4 mg dry weight of *K. petricola* was inoculated and the remaining three flasks were not inoculated thus representing the abiotic dissolution experiment. All experiments were run in triplicates. The Erlenmeyer flasks were placed in a climate chamber at constant temperature (25 °C), constant light source (90 µmol photons $m^{-2}\,s^{-1}$) and were shaken at 140 rpm min^{-1}. To support the fungus' carbon demand an additional 0.4 g of filter sterile glucose was added on day 65 of the experiment. The experiments were ran for 94 days.

Periodic sampling (5 ml) of the supernatant with a pipette while manually shaking the flask was done during the course of the experiment. The manual shaking was done to homogenise the components of the Erlenmeyer flasks, to have roughly similar amounts of mineral, liquid and biomass pipetted at each sampling interval and thus maintain a constant mineral:liquid:biomass ratio over the course of the experiment. Prior tests indicated a loss of about 0.05 g of olivine powder from the Erlenmeyer flask at each sampling point. The supernatant of the sampled aliquots were filtered with a 0.22 µm filter, and a part was used for pH measurement while the rest was acidified and stored at 4 °C for further elemental and isotopic analysis. The remaining solid phase consisting of biomass and olivine powder was used for quantitative polymerase chain reaction (PCR) analysis to measure fungal growth at each sampling point in the batch reactor.

2.3. Analysis

Fungal growth was determined by extracting the fungal DNA from

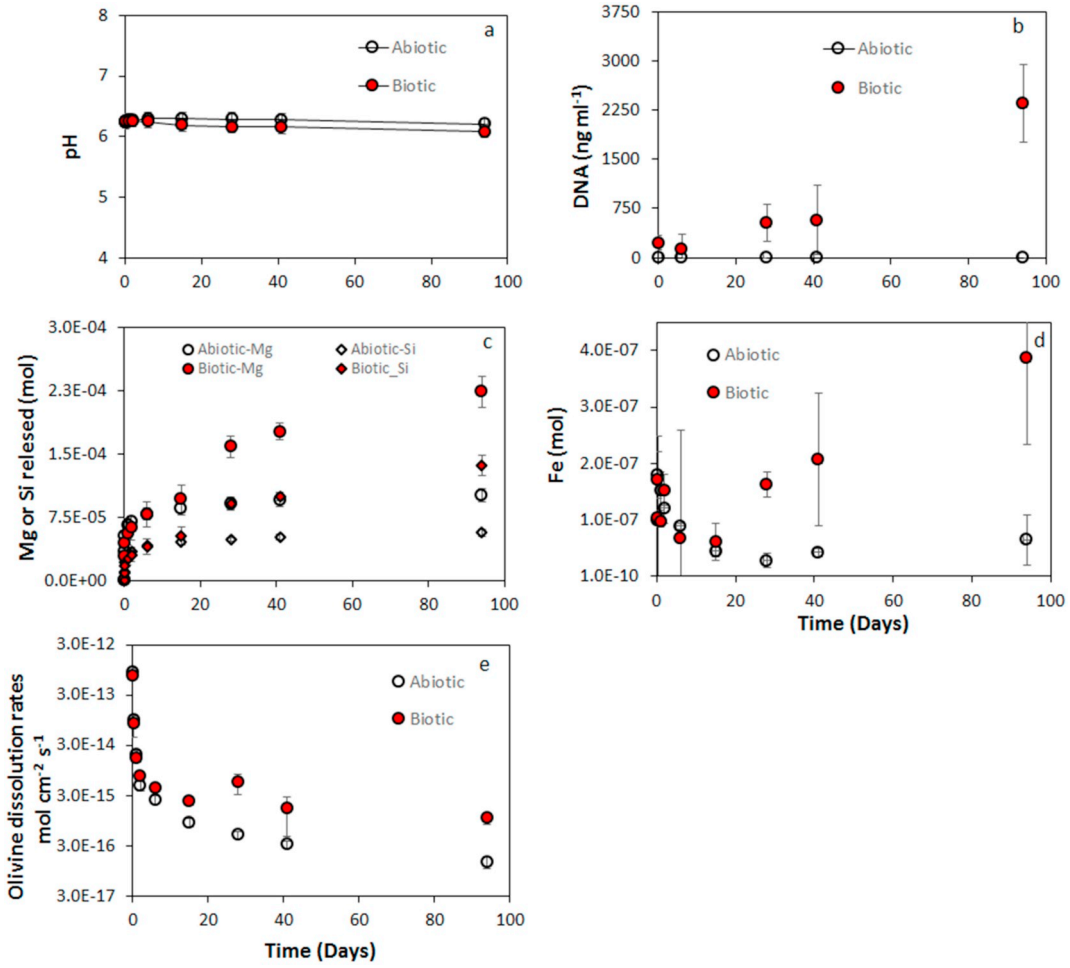

Fig. 1. Temporal evolution of a) pH; b) DNA concentration; c) Mg and Si released; d) Fe released; e) instantaneous olivine dissolution rates calculated from Mg concentrations (Eq. (1)) during dissolution experiments. The Y-axis of Figure (e) is plotted on a logarithmic scale of base 10. All uncertainty bars represent 2SD. 2SD on graph (a) represent analytical uncertainty, whereas on graphs b, c, d and e represents the analytical uncertainty for an individual measurement or uncertainty derived from the repeatability of three independent experiments, whichever was larger. For plots where no uncertainty is shown, the uncertainty is smaller than the symbols. See Table 1, Table S3 and Table S4 for detailed information.

the solid samples and quantifying the extracted DNA using quantitative PCR at BAM using the protocol of Martin-Sanchez et al. (2016). For a detailed description of the procedure the reader is referred to that article.

A part of the acidified supernatant sample was used for elemental analysis using Inductively Coupled Plasma Optical Emission Spectrometry (ICP-OES, Varian 720-ES) at the Helmholtz Laboratory for the Geochemistry of the Earth Surface (HELGES) at GFZ Potsdam (von Blanckenburg et al., 2016). The analysis was performed following the procedure described in Schuessler et al. (2016). Briefly, all samples and standards (ICP multi element solution) were diluted 1:3 using 0.3 M quartz-distilled HNO_3 acid and 1 mg/g Cs for matrix matching the samples to the calibration standards within 5% relative. Samples were doped with known concentrations of In and Sc to check for instrument stability during the measurements. A quality control solution (in 0.3 M HNO_3 and 1 mg/g Cs, made from Merck CertiPUR multi element standards with certified concentrations traceable to NIST reference materials) matrix-matched to that of the samples and solution was prepared. This solution and blanks were analyzed every 12 samples to assess measurement uncertainty and verify absence of contamination during the run. Based on repeated measurement of the quality control standards, the analytical uncertainty was estimated to be < 5.2%. See supporting information (Table S1) for details on quality controls samples preparation and analysis.

The Mg dissolution rate from the olivine mineral at each sampling interval was calculated following the mineral dissolution study by Daval et al. (2011).

$$r[t] = \frac{\Delta[i]}{SSA \times \Delta t \times \eta[i]} \quad (1)$$

where, r[t] is the dissolution rate (mol $cm^{-2} s^{-1}$) of olivine at time t, i.e. between two consecutive sampling points (calculated from supernatant Mg or Si concentrations); Δ[i] is the difference in molar amount of solute i (Mg or Si; mol) sampled between two sampling points; SSA is the specific surface area of the olivine (cm^2; due to experimental limitations we were not able to determine the changes in surface area induced by the presence of *K. petricola* or any structural changes in olivine during the course of the experiment. Therefore, we used the initial surface area of the olivine but accounted for the changes in the amount of olivine caused by pipetting at each sampling interval as explained in the method section); Δt is the time interval between two sampling points (s); η[i] is the stoichiometric coefficient ratio of solute i (1.86 for Mg and 1 for Si as measured by electron microprobe).

The Mg isotope composition of the initial bulk solid olivine and the acidified supernatant solutions (sampled at different times during the experiments) were determined by Multicollector Inductively Coupled Plasma Mass Spectrometry (MC-ICP-MS, Thermo Scientific Neptune) after Mg separation from the sample matrix. All samples and standards for Mg isotopes analysis were processed in the HELGES clean lab facility using ultrapure acids. Blanks and reference materials were processed in

parallel with the samples to quantify measurement accuracy and potential cross contamination. The reference materials Cambridge-1 and BHVO-2 were prepared in both pure and doped form. Doped solutions indicate that pure Mg solutions (500 ng/ml Mg) were doped in the input solution. The blanks, samples and reference material were first treated with a mixture of concentrated HNO_3, HCl, H_2O_2 and HF (HF was used only for dissolving olivine) on a hotplate at 150 °C in PFA vials. The samples were evaporated and re-dissolved multiple times in acids until completely dissolved. Finally the samples were dissolved in 1 M HNO_3 prior to Mg separation by cation exchange column chromatography. The protocols for the column separation procedure along with instrument settings for Mg isotopes analysis by MC-ICP-MS are given in Pokharel et al. (2017). Results are expressed in the δ-notation as the part per thousand (‰) deviation of the $^{26}Mg/^{24}Mg$ ratio from the international measurement standard DSM3, $\delta^{x}Mg_{sample} = [((^{x}Mg/^{24}Mg)_{sample}/(^{x}Mg/^{24}Mg)_{DSM3}) - 1 \times 1000]$, where x = 26 or 25. Based on repeated measurements of reference materials (both pure and doped), the uncertainty in $\delta^{26}Mg$ and $\delta^{25}Mg$ is estimated at ± 0.1‰ (2SD) and ± 0.06‰ (2SD), respectively. See supporting information for details on reference materials measurements and uncertainties (Table S2).

3. Results

Fig. 1 shows the evolution of pH, elemental Mg, Si, and Fe concentrations in the supernatant, fungal DNA analysis for estimating growth, and the olivine dissolution rate with experimental run time for both abiotic and biotic experiments. The pH was maintained constant at around 6.2 by the MES buffer for both abiotic and biotic experiments (Fig. 1a; Table 1). DNA analysis of the solid samples showed that fungal biomass increased: the DNA concentrations went from 230 to 2350 DNA ng/ml over the 94 days of the runs (Fig. 1b; Table 1). Despite the consistent pH between the biotic and abiotic experiments, the release of both Mg and Si varied between them: the biotic experiments liberated higher amounts of both these elements (Fig. 1c). In both experiments, there was a rapid initial release of both Mg and Si during the first two days, after which the release slowed down. Fe was initially released into the solution but was rapidly removed in the first 20 days in both experiments (Fig. 1d) - likely as Fe(III) precipitates. In the abiotic experiment, the amount of Fe remained constant in the solution after 20 days (slight changes were within the analytical uncertainty), whereas in the biotic experiment, the concentrations of dissolved Fe increased with time. Details of Mg, Si, and Fe concentrations in the supernatant along with the respective uncertainties are provided in the supporting information (Table S3). A constant dissolution rate for Mg and Si was not attained by the end of this experiment. Calculations using PHREEQC-2 (Parkhurst and Appelo, 1999) and the included llnl.dat database showed that Mg and Si were undersaturated in the bulk solution with respect to any Mg- or Si-bearing secondary minerals. The amount of Mg released from the olivine into solution was low, relative to the total amount of Mg in the solid olivine, for both abiotic and biotic experiments (0.75% and 1.65% respectively).

The olivine dissolution rate (Eq. (1)) calculated from Mg concentrations at the end of 94 days for the biotic experiment (1.04×10^{-15} mol cm^{-2} s^{-1}) was seven times higher than that of the abiotic dissolution experiment (1.43×10^{-16} mol cm^{-2} s^{-1}) (Table 1; Fig. 1e). Detailed calculation of the dissolution rates using the parameters in Eq. (1) is provided in the supporting information (Table S4).

All measured isotopic data showed mass-dependent isotope fractionation. Based on the slope in a three-isotope-plot (Young and Galy, 2004) and the deviation of $\delta^{25}Mg$ from the mass-dependent fractionation line typical for equilibrium fractionation ($\Delta^{25}Mg'$, Fig. 2b), an equilibrium isotope effect could not be singled-out from a kinetic effect from the slope of the mass-dependent fractionation line (Fig. 2a and b), given the uncertainty of these values and the low spread in $\delta^{26}Mg$. The temporal evolution of the Mg isotopic ratio of the supernatant did not differ between abiotic and biotic experiments, despite differences in the amounts of Mg released.

Both experiments showed an initial preferential release of ^{24}Mg over ^{26}Mg during the early stages of the experiment, but at the later stages $\delta^{26}Mg$ of the solution approached a value identical to the initial unreacted olivine (Fig. 3). Any possible differences in $\delta^{26}Mg$ of the solution between the abiotic and biotic experiment were within the analytical uncertainty of the MC-ICP-MS (± 0.1‰) and thus are not detectable. All $\delta^{26}Mg$ data for each of the independent experiments is presented in the supporting information (Table S3).

A similar picture emerged from the evolution of the supernatants Mg/Si ratios. Fig. 4 shows that the olivine dissolution can be separated into two stages: (i) an initial non-stoichiometric dissolution stage yielding a high Mg/Si ratio in the supernatant followed by (ii) a

Table 1
Summary of the results obtained for the abiotic and biotic dissolution experiments.

Experiment	Time (Days)	pH	DNA (ng/ ml)	± [b]2SD	Mg (moles)	± [b]2SD	[a]Olivine Dissolution Rates (mol cm^{-2} s^{-1})	± [b]2SD	$\delta^{25}Mg_{DSM3}$ (‰)	± [b]2SD	$\delta^{26}Mg_{DSM3}$ (‰)	± [b]2SD
Abiotic	0	6.21	0		0	0						
	0.04	6.24			3.44E-05	0.63E-05	8.74E-13	1.64E-13	−0.37	0.06	−0.71	0.13
	0.25	6.25			5.30E-05	0.50E-05	9.62E-14	2.70E-14	−0.31	0.06	−0.62	0.12
	1	6.28			6.61E-05	0.72E-05	1.90E-14	0.43E-14	−0.27	0.10	−0.54	0.18
	2	6.26			7.04E-05	0.65E-05	4.67E-15	1.05E-15	−0.26	0.06	−0.52	0.10
	6	6.30	0.004	0.008	7.91E-05	0.65E-05	2.43E-15	0.46E-15	−0.25	0.08	−0.50	0.16
	15	6.30			8.60E-05	0.76E-05	8.62E-16	1.62E-16	−0.22	0.06	−0.43	0.10
	28	6.29	0.034	0.067	9.15E-05	0.80E-05	4.89E-16	0.92E-16	−0.26	0.06	−0.49	0.10
	41	6.28	0.001	0.002	9.51E-05	0.80E-05	3.16E-16	0.60E-17	−0.23	0.06	−0.47	0.12
	94	6.20	0.008	0.015	1.02E-04	0.08E-04	1.43E-16	0.38E-16	−0.19	0.06	−0.38	0.10
Biotic	0	6.21	228	114	0							
	0.04	6.23			2.91E-05	0.50E-05	7.40E-13	1.39E-13	−0.36	0.07	−0.70	0.13
	0.25	6.25			4.45E-05	1.20E-05	7.95E-14	3.62E-14	−0.28	0.06	−0.54	0.10
	1	6.26			5.60E-05	1.36E-05	1.67E-14	0.31E-14	−0.27	0.13	−0.53	0.21
	2	6.26			6.26E-05	1.43E-05	7.28E-15	1.36E-15	−0.24	0.07	−0.48	0.10
	6	6.25	126	239	7.80E-05	1.49E-05	4.29E-15	0.80E-15	−0.29	0.06	−0.55	0.10
	15	6.19			9.68E-05	1.62E-05	2.36E-15	0.44E-15	−0.24	0.13	−0.46	0.23
	28	6.16	527	287	1.59E-04	0.13E-04	5.48E-15	2.35E-15	−0.23	0.09	−0.46	0.20
	41	6.15	535	574	1.77E-04	0.09E-04	1.61E-15	1.14E-15	−0.22	0.15	−0.44	0.27
	94	6.08	2304	571	2.24E-04	0.18E-04	1.04E-15	0.24E-15	−0.18	0.10	−0.36	0.19

[a] Instantaneous olivine dissolution rates calculated between two consecutive sampling points (calculated from supernatant Mg concentrations using Eq. (1)).
[b] 2SD represents the analytical uncertainty for an individual measurement or uncertainty derived from the repeatability of three independent experiments, whichever was larger (see Table S3 for all individual analyses).

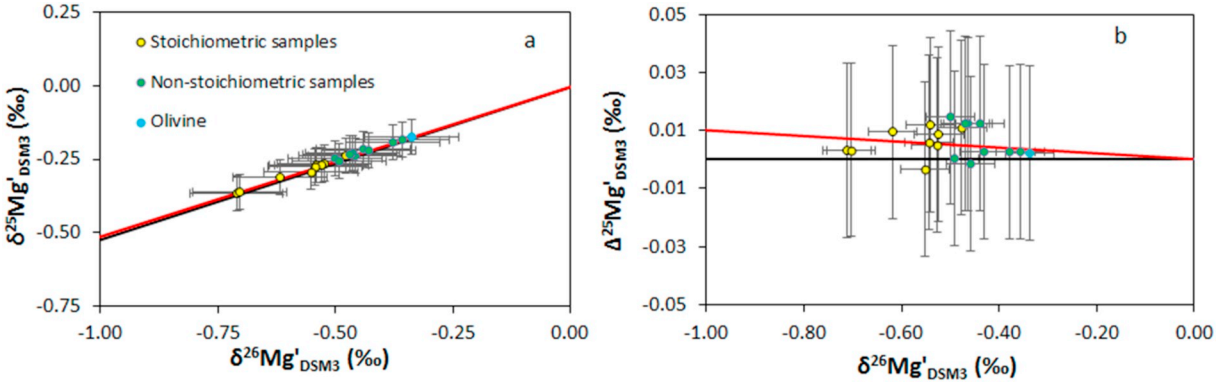

Fig. 2. Three-isotope plot diagram for samples measured in this study. The solid red line represents the kinetic fractionation line (slope = 0.511) and the solid black line represent the equilibrium fractionation line (slope = 0.521). For both graphs, yellow circles show the samples measured during the non-stoichiometric dissolution phase (up to day 2), green circles are the sample measured during the stoichiometric dissolution phase, and blue circle is the initial olivine. (a) $\delta^{26}Mg'_{DSM3}$ vs $\delta^{25}Mg'_{DSM3}$ plot as defined in Young and Galy (2004). Uncertainty in the plot are based on repeated measurement of reference materials processed through the Mg column chemistry and are ± 0.10‰ (2SD, $\delta^{26}Mg'_{DSM3}$) and ± 0.06‰ (2SD, $\delta^{25}Mg'_{DSM3}$). (b) $\Delta^{25}Mg'$ and $\delta^{26}Mg'$ graph for the samples. The uncertainty for $\Delta^{25}Mg'$ was ± 0.03 (1SD) and was based on Eq. (19) in Young and Galy (2004). The uncertainty for $\delta^{26}Mg'_{DSM3}$ was ± 0.05 (1SD). (For interpretation of the references to colour in this figure legend, the reader is referred to the web version of this article.)

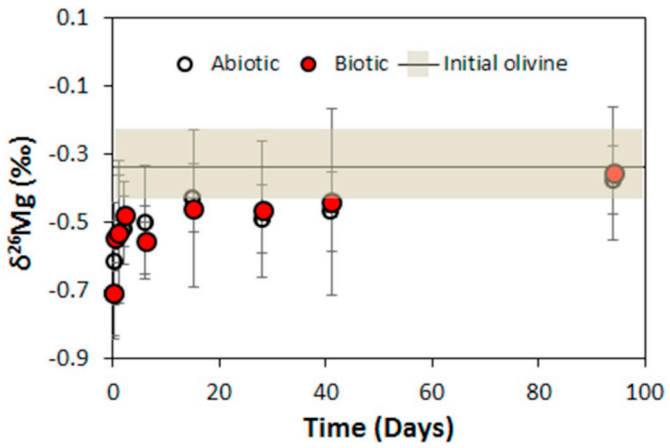

Fig. 3. Mg isotopic composition of the bulk dissolved phase for the abiotic and biotic experiments as a function of experiment run time. The error bars (2SD) in the graph was either derived from the analytical uncertainty from the individual measurements by MC-ICPMS or the uncertainty from the repeatability of independent growth experiments, whichever was larger. The Mg isotopic composition ($\delta^{26}Mg$) of the initial olivine was measured to be −0.34 ± 0.10‰ (2SD). The grey area represents the 2SD of $\delta^{26}Mg$ of the initial olivine.

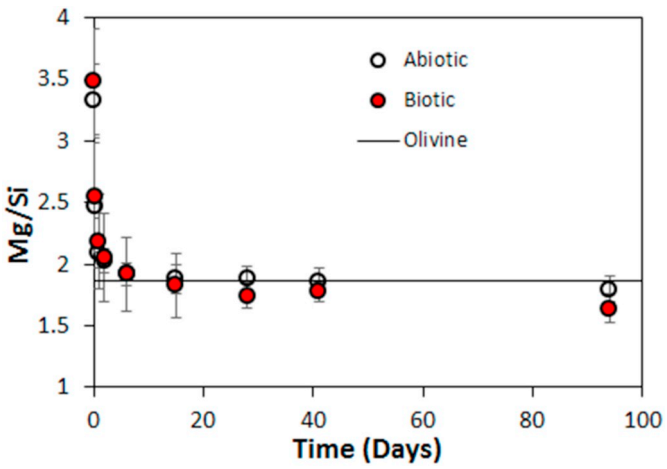

Fig. 4. Mg/Si molar ratio in the dissolved phase of the abiotic and biotic experiments, where the solid line denotes the molar Mg/Si ratio of initial olivine (1.86). The uncertainty in the figure is 2SD and is based on error propagation of uncertainties in measured Si and Mg concentrations.

stoichiometric stage yielding an Mg/Si ratio that was identical to Mg/Si of the dissolving olivine.

4. Discussion

4.1. Dissolution stages, processes and isotope fractionation

The olivine structure is made of individual silicon-tetrahedra linked by Mg atoms each of which are in octahedral coordination (Birle et al., 1968). At acidic conditions, protons are transported to the olivine surface either by diffusion or advection. The initial non-stoichiometric stage of dissolution is attributed to rapid exchange of protons with Mg^{2+} atoms in the olivine surface along with simultaneous polymerization of silica tetrahedra (Eq. (2)) (Daval et al., 2011; Johnson et al., 2014; Maher et al., 2016; Pokrovsky and Schott, 2000a; Pokrovsky and Schott, 2000b). The silica tetrahedra simultaneously dissolve as silicic acid (Eq. (3)) but with a slower reaction kinetics than the Mg^{2+} release hydrolysis reaction (Maher et al., 2016).

$$Mg_2SiO_4 + 4H^+ \rightarrow 2Mg^{2+} + SiO_2 + 2H_2O \quad (2)$$

$$SiO_2 + 2H_2O \rightarrow H_4SiO_4\,(aq) \quad (3)$$

Due to the differences in reaction kinetics for Mg and Si release, Mg is depleted in the surface of olivine in comparison to amorphous Si. The measured high Mg/Si molar ratio (in comparison to the stoichiometric molar ratio of the unreacted olivine) in the bulk solution during the initial non-stoichiometric phase confirms this (Fig. 4). The formed surface layer thus is low in Mg and high in Si, and has been previously termed as the “active layer” or the “leached layer” (Maher et al., 2016; Pokrovsky and Schott, 2000a). We refer to this surface layer as “Si-rich amorphous layer”. Hellmann et al. (2012) proposed a different mechanism whereby interfacial dissolution/precipitation processes take place at the thin-fluid film in between the amorphous silica layer and the crystalline olivine. They postulated that the chemistry of this thin-fluid film differs from the bulk solution, and thus in this layer the precipitation of amorphous silica takes place even if the bulk solution is undersaturated with respect to amorphous silica. Regardless of the mode of formation of this layer, once the Si-rich amorphous layer has formed, the dissolution of surface silica is always governed by reaction 3 (Maher et al., 2016).

We thus infer that in the initial non-congruent dissolution phase such a Si-rich amorphous surface layer is formed and Mg is not any

further present at the surface for protonation. The Si-rich amorphous layer can slow down the release of Mg and Si, thereby significantly decreasing the olivine dissolution rates. The parabolic nature of the dissolution rate curve observed is due to this effect (Fig. 1d). As these surface layer are porous, protons can diffuse through this layer onto the olivine surface (Pokrovsky and Schott, 2000a). The dissolution rate at this stage is therefore controlled by transport through the Si-rich amorphous layer. As the proton reacts with the crystalline olivine in the interior boundary of the amorphous layer, Mg^{2+} is released (following Eq. (2)) and diffuses through the porous surface layer into the solution. Simultaneously new Si tetrahedra are released by H^+ at the inner edge of the amorphous surface layer. In the stoichiometric phase the Si release from the olivine surface balances the rate of dissolution of the external amorphous Si layer (following Eq. (3)) which thus maintains constant thickness (Hellmann et al., 2012; Maher et al., 2016). The Si-rich amorphous layer moves inward at a rate controlled by both the rate of Mg exchange according to the reaction given in Eq. (2) and the net release of Si via the reaction given in Eq. (3), resulting in stoichiometric release of these two elements (Fig. 4) (Maher et al., 2016). We observed a decrease in the olivine dissolution rates as the reaction progressed from initial non-stoichiometric to the stoichiometric stage (Fig. 1d) that amounted to two to three orders of magnitude. A similar decrease was observed by Daval et al. (2011) in solutions undersaturated in both Mg and Si.

The molar ratio of Fe/Mg in the supernatant was non-stoichiometric with respect to the initial olivine over the course of both biotic and abiotic experiments (Table S3). The Fe/Mg ratios in the supernatants were 1–2 orders of magnitude lower than the initial olivine ratio of 0.1. This incongruent release of Fe and Mg from the surface of olivine might be due to oxidation of Fe(II) released from olivine followed by precipitation due to the low solubility of Fe(III). During the non-stoichiometric dissolution phase the precipitation of Fe(III) phases is indicated by the decrease in the dissolved Fe amount in the solution (Fig. 1d). This Fe was released from the fayalite component of olivine initially as Fe(II) which upon entering the solution was fast oxidized to insoluble Fe(III) which was precipitated as Fe(III)oxy-hydroxides. Past studies have indicated that Fe(III) precipitates contribute to additional protection in the Si-rich amorphous layer and reduce the porosity of the layer by clogging (Saldi et al., 2013; Schott and Berner, 1983; Sissmann et al., 2013; Torres et al., 2014). Their presence thus potentially slows down olivine dissolution even further.

Within this framework we now explore the causes of the faster Mg and Si release in the presence of *K. petricola*. Fungi are known to break mineral structures by two mechanisms, 1) biomechanical weathering; and 2) biochemical weathering (Adeyemi and Gadd, 2005; Balogh-Brunstad et al., 2008; Bonneville et al., 2009; Callot et al., 1987; Chizhikova et al., 2016; Daghino et al., 2010; Duane, 2006; Gadd, 2007; Gadd, 2010; Hirsch et al., 1995; Hoffland et al., 2004; Krumbein and Jens, 1981). Both these processes are triggered by physical attachment of *K. petricola* to the mineral surface. Biomechanical weathering is caused by fungal hyphae penetration into weak spots of rocks like cracks and mineral cleavage to acquire nutrients. After attachment, fungal hyphae can generate an internal turgor pressure as high of 0.4 MPa (4 bars) to 8 MPa (80 bars) through osmosis that facilitates them to penetrate hard rock surfaces (Bechinger et al., 1999; Bonneville et al., 2009; Harold, 2002). However, *K. petricola* has a short hyphae with smaller surface area that limits its biomechanical weathering ability. Hence in *K. petricola* it is the biochemical weathering processes that have a greater influence on releasing metals from the rock surface. Biochemical fungal weathering is thought to take place by two processes, (I) proton-based and (II) ligand-based (Gadd, 2007; Gadd, 2010; Hoffland et al., 2004). Protons acidify the microenvironment of the fungi. They are excreted through the plasma membrane as H^+-ATPase, are produced from carbonic acid as a by-product of respiration, or are produced from organic acids (Balogh-Brunstad et al., 2008; Bonneville et al., 2009; Burford et al., 2003a). Pokharel et al. (2017) showed that in unbuffered conditions *K. petricola* lowered the pH of the growth solution by 3–4 units over the course of only a few days. Although in our experiment the MES buffer stabilized the pH of the solution, we speculate that a local pH change might have arisen that acidified the surface of the mineral in direct contact with *K. petricola*. Ligand-based weathering processes include release of for example siderophores, carboxylic acids, amino acids, phenolic compounds that potentially complex metals from the mineral surfaces (Gadd, 2007; Gadd, 2010; Hoffland et al., 2004). Through all these reactions weathering rates are accelerated at the zone of contact between mineral and fungi (Balogh-Brunstad et al., 2008; Li et al., 2016).

The similarity between both experiments in the early stages of the dissolution experiment indicates that the abiotic incongruent dissolution dominates the initial phase of dissolution. Measured DNA amounts show slow fungal growth during this period. In both experiments the initial formation of the amorphous Si surface layer appears to limit the rate of Mg release, and this process appears to be insensitive to the presence of the fungus. However, after 20 days cell numbers as quantified by the amount of DNA (Fig. 1c) increase substantially, and accelerate the release of Mg and Si in comparison to the abiotic experiments (Fig. 4). Although the presence of *K. petricola* enhances the release of Mg and Si, the release is still congruent in terms of $^{26}Mg/^{24}Mg$ and stoichiometric in terms of Mg/Si as in the abiotic experiments. We speculate that *K. petricola* acidifies the micro-environment of the mineral, supplying more protons to diffuse through the Si-rich amorphous layer. This additional provision of protons by *K. petricola* accelerates the olivine dissolution rate which however follows the same net reactions for congruent Mg and Si release as in the abiotic process previously described. We note that the Fe amount in the bulk solution increases in the later phase of the biotic experiment. The Fe release in the presence of *K. petricola* could be either due to the dissolution of the Fe(III) phase by micro-environment acidification of the Si-rich amorphous layer, or to the release of siderophores to form soluble Fe(III) complexes. Regardless of the cause, the dissolution of precipitated Fe(III) phases increases the permeability of the of Si-rich amorphous layer. This increased permeability, induced by the presence of *K. petricola,* in turn contributes to the faster olivine dissolution in the biotic experiment.

Despite the differences in dissolution rate the isotopic composition of the bulk solution did not differ between the abiotic and biotic experiment. The initial enrichment of ^{24}Mg in the growth solution indicates preferential release of light Mg isotopes during the proton exchange reactions (Eq. (2)). Maher et al. (2016) have suggested that the initial release of the ^{24}Mg during forsterite dissolution is due to preferential breaking of weaker $^{24}Mg—O$ bonds in comparison to a stronger $^{26}Mg—O$ bonds. A similar interpretation was suggested for the preferential release of light Mg isotopes during dissolution of the mineral hydromagnesite (Oelkers et al., 2018a). Therefore, this preferred release of light ^{24}Mg over ^{26}Mg is attributed to a surface kinetic effect where the irreversible detachment of Mg in the active layer (Eq. (2)) is a fast forward reaction entailing this isotope effect (Maher et al., 2016). As stated in Section 3 an equilibrium isotope effect could not be resolved from a kinetic effect from the slope of the mass-dependent fractionation line (Fig. 2a and b). When the dissolution reaction progresses towards the stoichiometric Mg and Si release stage, the isotopic composition of the bulk solution approaches that of bulk olivine too (Fig. 3). At this stage, steady-state dissolution develops, where the dissolution of ^{26}Mg outwards in the active layer counterbalances the preferential release of ^{24}Mg inwards in the layer. This counterbalancing of initial light isotope release by a heavy isotope later has also been observed for Fe, Mg and Si during mineral dissolution reactions at conditions of dynamic equilibrium (Brantley et al., 2004; DePaolo, 2011; Wiederhold et al., 2006; Wimpenny et al., 2010; Ziegler et al., 2005). We can exclude that the shift towards high $\delta^{26}Mg$ is due to uptake of Mg by the fungus. First, Pokharel et al. (2017) has observed that *K. petricola* incorporates heavier Mg isotope from the growth

solution, which is the opposite direction. Secondly, Pokharel et al. (2017) showed that a gram of dry cells of *K. petricola* incorporates about 365 μg of Mg. Considering that the dry weight of *K. petricola* at the end of 94 days was only about 41 mg indicates that the amount of Mg uptake by the fungi from the growth solution is negligible (< 1%) when compared to the amount released by olivine. To summarize, that the temporal evolution of the chemistry and the isotope ratios released do not differ between the biotic and the abiotic dissolution experiment shows that the fungus does not directly affect the release of Mg. That the release rates differ nevertheless shows that it is the interaction of the fungus with the amorphous silica layer that indirectly accelerates olivine dissolution.

4.2. Comparing olivine dissolution rates

Literature data (laboratory experimental studies and review articles) on abiotic olivine dissolution rates measured at near neutral pH (6–8), average Earth surface temperature (19 °C to 25 °C) and under low CO_2 conditions, range from 10^{-14}–$10^{-16.4}$ mol cm^{-2} s^{-1} (Brantley et al., 2008; Crundwell, 2014; Gislason et al., 2014; Golubev et al., 2005; Luce et al., 1972; Pokrovsky and Schott, 2000b; Renforth et al., 2015; Rimstidt et al., 2012; Wogelius and Walther, 1991), whereas the dissolution rates measured in our experiments in the congruent phase are 10^{-15} mol cm^{-2} s^{-1} for the biotic and 10^{-16} mol cm^{-2} s^{-1} for the abiotic experiment. However, it is important to discuss whether mineral weathering rates calculated from a short-term (< 1 yr) controlled laboratory experiment can be used to predict weathering rates in the complex environment of the Earth's surface. Comparison between laboratory and field silicate mineral weathering rates shows significant differences, with laboratory experiment typically being orders of magnitude higher than field rates (Gruber et al., 2014; White and Brantley, 2003). Differences in parameters like surface area, solution composition, fluid residence time, and covering of primary by secondary minerals cause these discrepancies. Also the presence of organisms can induce such differences. Oelkers et al. (2015) conducted a 5 year long forsterite mineral dissolution. The results showed that dissolution of forsterite is slowed by an order of magnitude from the short-term dissolution rates and they attributed this to the growth of microbial communities on the surface of olivine. The second observation of that study was that the batch solution isotope composition was isotopically heavier in Mg than the dissolving forsterite, a contradiction from what is typically observed in short-term laboratory experiments and field sites. The contradicting nature of these observations question whether, and what type of closed-system laboratory batch experiment setup correctly represent processes taking place in natural field settings that evolve over thousands of years.

4.3. Implications for soil pore water isotope composition

Weathering isotope models typically assume isotopically congruent dissolution over time scales of decades to millennia over which soil formation, weathering and erosion shape landscapes, meaning that solutes released from primary minerals obtain the isotope ratios of the primary mineral (Bouchez et al., 2013). At the first sight the initial release of Mg low in δ^{26}Mg found in this and other studies (Maher et al., 2016; Wimpenny et al., 2010) seems to invalidate this assumption. Further, in most weathering settings the dissolved Mg in soil pore water and rivers tends to be slightly lower in δ^{26}Mg relative to the dissolving rock (Mavromatis et al., 2014; Opfergelt et al., 2014; Tipper et al., 2010; Uhlig et al., 2017), which apparently supports incongruent release of light Mg isotopes. However, it is likely that this fractionation occurs during clay formation where the heavier Mg isotopes are preferentially incorporated into the clay structure (Ryu et al., 2016; Wimpenny et al., 2014), or by uptake of Mg into higher plants and/or fungi (Black et al., 2008; Bolou-Bi et al., 2010; Kimmig et al., 2018; Pokharel et al., 2017; Uhlig et al., 2017). However, the experimental results in this and in previous studies (mentioned above) also show that the initial isotope effect subsides after a few days or weeks. Hence, it is more likely that during slow natural weathering processes steady state mineral dissolution is attained over long time scales. Only during very low fluid/rock ratios and initial exposure of mineral surfaces to solutions, such as in deep fracture flow or in minerals or aquifers used for CO_2 sequestration might this effect become apparent.

4.4. Implications for CO_2 storage

Artificial dispersal of silicate mineral like olivine onto the Earth's surface or injection of CO_2 into ultramafic rock structures has been proposed as a means of CO_2 sequestration ("enhanced weathering") (Johnson et al., 2014; Moosdorf et al., 2014; Renforth et al., 2015; Schuiling et al., 1986; Schuiling and Krijgsman, 2006; Taylor et al., 2015). The formation of an amorphous Si layer significantly decreases release of Mg from the olivine mineral, hence limiting the pool of readily available Mg^{2+} for storage of CO_2 through carbonation reactions. However our short-term laboratory experiment indicates that the presence of *K. petricola* accelerated Mg release rates by a factor of seven in comparison to the abiotic controls. If valid over the 100 years scale of CO_2 sequestration our results suggest the that addition of a rock-inhabiting black fungus with the ground olivine in the "enhanced weathering" settings at Earth's surface temperature could provide a more efficient way to withdraw CO_2 from the atmosphere.

5. Conclusion

Laboratory dissolution experiments with the black fungus *K. petricola* enhanced olivine dissolution rates seven times over those in the abiotic controls. Despite faster Mg and Si release, the biotic experiment followed the same trend as the abiotic experiment in terms of the initial non-stoichiometric to the later stoichiometric Mg and Si release from the dissolving olivine, and the initial preferential release of isotopically light Mg to the later release of Mg that is isotopically congruent in its ^{26}Mg/^{24}Mg ratio. The initial non-stoichiometric phase was attributed to rapid exchange of Mg^{2+} with H^+ along with simultaneous polymerization of Si tetrahedra causing higher dissolution rates, whereas the stoichiometric phase was influenced by the buildup of the Si-rich amorphous layer that slowed the dissolution rates. The absence of differences in the temporal evolution of both the Mg/Si released and isotope ratio of the Mg released between the biotic and abiotic experiment indicates that in the presence of the fungi, olivine dissolves in the same way as in the abiotic process. We suggest the accelerated dissolution rate during the stoichiometric phase in the presence of *K. petricola* is due to provision of additional protons by fungal biochemical processes that acidify the micro-environment of the Si-rich amorphous surface layer to which *K. petricola* is attached. These additional protons will diffuse inwards into the amorphous Si layer where they react with the olivine surface, and eventually release Mg and Si into the solution. Our results also indicate that the presence of Fe precipitates in the Si-rich amorphous phase retards olivine dissolution rates. Through biomechanical and biochemical mechanism *K. petricola* dissolves the Fe precipitates, thereby making the Si-rich amorphous layer more porous which increases the olivine dissolution rates. Our Mg isotope study shows a distinct initial phase of ^{24}Mg release and indicates that Mg isotopes can trace incipient rock weathering. The enhanced biotic dissolution rates suggest that the presence of a rock-dissolving fungus in weathering settings or in CO_2 sequestration experiments may aid to accelerate CO_2 binding.

Funding

This research was supported by the ISONOSE Marie Curie Research training network funded from the People Programme (Marie Curie Actions) of the European Union's Seventh Framework Programme FP7/

2007-2013/under REA grant agreement n° (608068).

Acknowledgements

We want to thank Prof. Dr. Anna Gorbushina from BAM for providing the strain of the fungus as well as allowing us to conduct the experiments at her laboratory. From the GFZ research group at GFZ Potsdam, we gratefully acknowledge Josefine Buhk and Jutta Schlegel for help during clean lab sample preparation and Mg isotope measurements. We also want to acknowledge Prof. Dr. Ralf Milke from FU Berlin for Electron microprobe analysis and Carsten Prinz from BAM Berlin for BET analysis. We thank the Editor Prof. Michael Böttcher and the anonymous reviewer for their constructive comments.

Appendix A. Supplementary data

Supplementary data to this article can be found online at https://doi.org/10.1016/j.chemgeo.2019.07.001.

References

Adeyemi, A.O., Gadd, G.M., 2005. Fungal degradation of calcium-, lead- and silicon-bearing minerals. Biometals, 18(3): 269–281, doi:https://doi.org/10.1007/s10534-005-1539-2 http://dx.doi.org/10.1007/s10534-005-1539-2.

Balland-Bolou-Bi, C., Bolou-Bi, E.B., Vigier, N., Mustin, C., Poszwa, A., 2019. Increased Mg release rates and related Mg isotopic signatures during bacteria-phlogopite interactions. Chem. Geol., 506: 17–28, doi:https://doi.org/10.1016/j.chemgeo.2018.12.020https://doi.org/10.1016/j.chemgeo.2018.12.020.

Balogh-Brunstad, Z. et al., 2008. Biotite weathering and nutrient uptake by ectomycorrhizal fungus, Suillus tomentosus, in liquid-culture experiments. Geochim. Cosmochim. Acta, 72(11): 2601–2618, doi:https://doi.org/10.1016/j.gca.2008.04.003http://dx.doi.org/10.1016/j.gca.2008.04.003.

Banfield, J.F., Barker, W.W., Welch, S.A., Taunton, A., 1999. Biological impact on mineral dissolution: application of the lichen model to understanding mineral weathering in the rhizosphere. Proc. Natl. Acad. Sci., 96(7): 3404–3411, doi:https://doi.org/10.1073/pnas.96.7.3404http://dx.doi.org/10.1073/pnas.96.7.3404.

Bechinger, C. et al., 1999. Optical Measurements of Invasive Forces Exerted by Appressoria of a Plant Pathogenic Fungus. Science, 285(5435): 1896, doi:https://doi.org/10.1126/science.285.5435.1896http://dx.doi.org/10.1126/science.285.5435.1896.

Birle, J.D., Gibbs, G.V., Moore, P.B., Smith, J.V., 1968. Crystal structures of natural olivines. Am. Mineral. 53 (5–6), 807–824.

Black, J., Epstein, Emanuel, Rains, William D., Yin, Q.-z., Casey, W.H., 2008. Magnesium-isotope fractionation during plant growth. Environmental Science & Technology 42 (21), 7831–7836. https://doi.org/10.1021/es8012722.

von Blanckenburg, F., Wittmann, H., Schuessler, J.A., 2016. HELGES: Helmholtz Laboratory for the Geochemistry of the Earth Surface. Journal of large-scale research facilities 2, A84. https://doi.org/10.17815/jlsrf-2-141.

Bolou-Bi, E.B., Poszwa, A., Leyval, C., Vigier, N., 2010. Experimental determination of magnesium isotope fractionation during higher plant growth. Geochim. Cosmochim. Acta, 74(9): 2523–2537, doi:https://doi.org/10.1016/j.gca.2010.02.010http://dx.doi.org/10.1016/j.gca.2010.02.010.

Bolou-Bi, E.B., Vigier, N., Poszwa, A., Boudot, J.-P., Dambrine, E., 2012. Effects of biogeochemical processes on magnesium isotope variations in a forested catchment in the Vosges Mountains (France). Geochim. Cosmochim. Acta, 87: 341–355, doi:https://doi.org/10.1016/j.gca.2012.04.005http://dx.doi.org/10.1016/j.gca.2012.04.005.

Bonneville, S. et al., 2009. Plant-driven fungal weathering: early stages of mineral alteration at the nanometer scale. Geology, 37: 4, doi:https://doi.org/10.1130/g25699a.1 https://doi.org/10.1130/g25699a.1

Bonneville, S. et al., 2011. Tree-mycorrhiza symbiosis accelerate mineral weathering: evidences from nanometer-scale elemental fluxes at the hypha–mineral interface. Geochim. Cosmochim. Acta, 75(22): 6988–7005, doi:https://doi.org/10.1016/j.gca.2011.08.041http://dx.doi.org/10.1016/j.gca.2011.08.041.

Bouchez, J., von Blanckenburg, F., Schuessler, J.A., 2013. Modeling novel stable isotope ratios in the weathering zone. Am. J. Sci., 313(4): 267–308, doi:https://doi.org/10.2475/04.2013.01http://dx.doi.org/10.2475/04.2013.01.

Brantley, S.L. et al., 2004. Fe isotopic fractionation during mineral dissolution with and without bacteria1. Geochim. Cosmochim. Acta, 68(15): 3189–3204, doi:10.1016/j.gca.2004.01.023http://dx.doi.org/10.1016/j.gca.2004.01.023.

Brantley, S., Kubicki, J., F White, A., 2008. Kinetics of Water-Rock Interaction. Springer, New York, NY, doi:https://doi.org/10.1007/978-0-387-73563-4http://dx.doi.org/10.1007/978-0-387-73563-4.

Burford, E.P., Fomina, M., Gadd, G.M., 2003a. Fungal involvement in bioweathering and biotransformation of rocks and minerals. Mineral. Mag., 67(6): 1127–1155, doi:https://doi.org/10.1180/0026461036760154http://dx.doi.org/10.1180/0026461036760154.

Burford, E.P., Kierans, M., Gadd, G.M., 2003b. Geomycology: fungi in mineral substrata. Mycologist, 17(3): 98–107, doi:https://doi.org/10.1017/S0269-915X(03)00311-2 http://dx.doi.org/10.1017/S0269-915X(03)00311-2.

Callot, G., Maurette, M., Pottier, L., Dubois, A., 1987. Biogenic etching of microfractures in amorphous and crystalline silicates. Nature, 328: 147, doi:https://doi.org/10.1038/328147a0http://dx.doi.org/10.1038/328147a0.

Chizhikova, N., Lessovaia, S., Gorbushina, A., 2016. Biogenic Weathering of Mineral Substrates (Review). Biogenic – Abiogenic Interactions in Natural and Anthropogenic Systems Springerhttps://doi.org/10.1007/978-3-319-24987-2_2. 7-14 pp.

Crundwell, F.K., 2014. The mechanism of dissolution of forsterite, olivine and minerals of the orthosilicate group. Hydrometallurgy, 150: 68–82, doi:https://doi.org/10.1016/j.hydromet.2014.09.006https://doi.org/10.1016/j.hydromet.2014.09.006.

Daghino, S., Martino, E., Perotto, S., 2010. Fungal Weathering and Implications in the Solubilization of Metals from Soil and from Asbestos Fibres. (329-338 pp).

Daval, D. et al., 2011. Influence of amorphous silica layer formation on the dissolution rate of olivine at 90 °C and elevated pCO2. Chem. Geol., 284(1): 193–209, doi:https://doi.org/10.1016/j.chemgeo.2011.02.021https://doi.org/10.1016/j.chemgeo.2011.02.021.

DePaolo, D.J., 2011. Surface kinetic model for isotopic and trace element fractionation during precipitation of calcite from aqueous solutions. Geochim. Cosmochim. Acta, 75(4): 1039–1056, doi:https://doi.org/10.1016/j.gca.2010.11.020http://dx.doi.org/10.1016/j.gca.2010.11.020.

Duane, M.J., 2006. Coeval biochemical and biophysical weathering processes on Quaternary sandstone terraces south of Rabat (Temara), northwest Morocco. Earth Surf. Process. Landf., 31(9): 1115–1128, doi:https://doi.org/10.1002/esp.1313https://doi.org/10.1002/esp.1313.

Ehrlich, H.L., 1996. How microbes influence mineral growth and dissolution. Chem. Geol., 132(1): 5–9, doi:https://doi.org/10.1016/S0009-2541(96)00035-6https://doi.org/10.1016/S0009-2541(96)00035-6.

Fahad, Z.A., Bolou-Bi, E.B., Köhler, S.J., Finlay, R.D., Mahmood, S., 2016. Fractionation and assimilation of Mg isotopes by fungi is species dependent. Environ. Microbiol. Rep., 8(6): 956–965, doi:https://doi.org/10.1111/1758-2229.12459https://doi.org/10.1111/1758-2229.12459

Fries, D.M. et al., 2019. The response of Li and Mg isotopes to rain events in a highly-weathered catchment. Chem. Geol., 519: 68–82, doi:https://doi.org/10.1016/j.chemgeo.2019.04.023https://doi.org/10.1016/j.chemgeo.2019.04.023.

Gadd, G.M., 2007. Geomycology: biogeochemical transformations of rocks, minerals, metals and radionuclides by fungi, bioweathering and bioremediation. Mycol. Res., 111(1): 3–49, doi:https://doi.org/10.1016/j.mycres.2006.12.001http://dx.doi.org/10.1016/j.mycres.2006.12.001.

Gadd, G.M., 2010. Metals, minerals and microbes: geomicrobiology and bioremediation. Microbiology, 156: 609–643, doi:https://doi.org/10.1099/mic.0.037143-0https://doi.org/10.1099/mic.0.037143-0

Gislason, S.R. et al., 2014. Rapid solubility and mineral storage of CO2 in basalt. Energy Procedia, 63: 4561–4574, doi:https://doi.org/10.1016/j.egypro.2014.11.489https://doi.org/10.1016/j.egypro.2014.11.489.

Golubev, S.V., Pokrovsky, O.S., Schott, J., 2005. Experimental determination of the effect of dissolved CO2 on the dissolution kinetics of Mg and Ca silicates at 25 °C. Chem. Geol., 217(3): 227–238, doi:https://doi.org/10.1016/j.chemgeo.2004.12.011https://doi.org/10.1016/j.chemgeo.2004.12.011.

Gorbushina, A.A., Kotlova, E.R., Sherstneva, O.A., 2008. Cellular responses of microcolonial rock fungi to long-term desiccation and subsequent rehydration. Stud. Mycol., 61(1): 91–97, doi:https://doi.org/10.3114/sim.2008.61.09 http://dx.doi.org/10.3114/sim.2008.61.09.

Gruber, C., Zhu, C., Georg, R.B., Zakon, Y., Ganor, J., 2014. Resolving the gap between laboratory and field rates of feldspar weathering. Geochim. Cosmochim. Acta, 147: 90–106, doi:https://doi.org/10.1016/j.gca.2014.10.013https://doi.org/10.1016/j.gca.2014.10.013.

Hagerberg, D., Thelin, G., Wallander, H., 2003. The production of ectomycorrhizal mycelium in forests: relation between forest nutrient status and local mineral sources. Plant Soil, 252(2): 279–290, doi:https://doi.org/10.1023/a:1024719607740https://doi.org/10.1023/a:1024719607740

Harley, J.L., Smith, S.E., 1983. Mycorrhizal Symbiosis, 22. Academic Press Inc., London; New York, USA, x + 483 pp. pp, doi:https://doi.org/10.1017/s0014479700014113 https://doi.org/10.1017/s0014479700014113

Harold, F.M., 2002. Force and compliance: rethinking morphogenesis in walled cells. Fungal genetics and biology: FG & B, 37(3): 271–282, doi:https://doi.org/10.1016/s1087-1845(02)00528-5https://doi.org/10.1016/s1087-1845(02)00528-5.

Hawksworth, D.L., 1988. The variety of fungal-algal symbioses, their evolutionary significance, and the nature of lichens. Bot. J. Linn. Soc., 96(1): 3–20, doi:https://doi.org/10.1111/j.1095-8339.1988.tb00623.xhttps://doi.org/10.1111/j.1095-8339.1988.tb00623.x.

Hellmann, R. et al., 2012. Unifying natural and laboratory chemical weathering with interfacial dissolution–reprecipitation: a study based on the nanometer-scale chemistry of fluid–silicate interfaces. Chem. Geol., 294–295(0): 203–216, doi:https://doi.org/10.1016/j.chemgeo.2011.12.002http://dx.doi.org/10.1016/j.chemgeo.2011.12.002.

Henderson, M.E.K., Duff, R.B., 1963. The release of metallic and silicate ions from minerals, rocks, and soils by fungal activity. J. Soil Sci., 14(2): 236–246, doi:https://doi.org/10.1111/j.1365-2389.1963.tb00949.xhttps://doi.org/10.1111/j.1365-2389.1963.tb00949.x.

Hirsch, P., Eckhardt, F.E.W., Palmer Jr, R.J., 1995. Fungi active in weathering of rock and stone monuments. Can. J. Bot., 73 (S1): 1384–1390, doi:https://doi.org/10.1139/b95-401https://doi.org/10.1139/b95-401.

Hoffland, E. et al., 2004. The role of fungi in weathering. Front. Ecol. Environ., 2(5): 258–264, doi:https://doi.org/10.1890/1540-9295(2004)002[0258:TROFIW]2.0.CO;2https://doi.org/10.1890/1540-9295(2004)002[0258:TROFIW]2.0.CO;2.

Johnson, N.C. et al., 2014. Olivine dissolution and carbonation under conditions relevant

for in situ carbon storage. Chem. Geol., 373: 93–105, doi:https://doi.org/10.1016/j.chemgeo.2014.02.026https://doi.org/10.1016/j.chemgeo.2014.02.026.
Kimmig, S.R., Holmden, C., Bélanger, N., 2018. Biogeochemical cycling of Mg and its isotopes in a sugar maple forest in Québec. Geochim. Cosmochim. Acta, 230: 60–82, doi:https://doi.org/10.1016/j.gca.2018.03.020https://doi.org/10.1016/j.gca.2018.03.020.
Kolesov, B.A., Geiger, C.A., 2004. A Raman spectroscopic study of Fe–Mg olivines. Phys. Chem. Miner., 31(3): 142–154, doi:https://doi.org/10.1007/s00269-003-0370-yhttps://doi.org/10.1007/s00269-003-0370-y.
Krumbein, W.E., Jens, K., 1981. Biogenic rock varnishes of the negev desert (Israel) an ecological study of iron and manganese transformation by cyanobacteria and fungi. Oecologia, 50(1): 25–38, doi:https://doi.org/10.1007/bf00378791https://doi.org/10.1007/bf00378791.
Li, Z., Liu, L., Chen, J., Teng, H., 2016. Cellular dissolution at hypha- and spore-mineral interfaces revealing unrecognized mechanisms and scales of fungal weathering. Geology, 44(4): 319–322, doi:https://doi.org/10.1130/g37561.1https://doi.org/10.1130/g37561.1
Luce, R.W., Bartlett, R.W., Parks, G.A., 1972. Dissolution kinetics of magnesium silicates. Geochim. Cosmochim. Acta, 36(1): 35–50, doi:https://doi.org/10.1016/0016-7037(72)90119-6https://doi.org/10.1016/0016-7037(72)90119-6.
Maher, K. et al., 2016. A spatially resolved surface kinetic model for forsterite dissolution. Geochim. Cosmochim. Acta, 174: 313–334, doi:https://doi.org/10.1016/j.gca.2015.11.019http://dx.doi.org/10.1016/j.gca.2015.11.019.
Martin-Sanchez, P.M., Gorbushina, A.A., Kunte, H.-J., Toepel, J., 2016. A novel qPCR protocol for the specific detection and quantification of the fuel-deteriorating fungus Hormoconis resinae. Biofouling, 32(6): 635–644, doi:https://doi.org/10.1080/08927014.2016.1177515https://doi.org/10.1080/08927014.2016.1177515
Mavromatis, V., Prokushkin, A.S., Pokrovsky, O.S., Viers, J., Korets, M.A., 2014. Magnesium isotopes in permafrost-dominated Central Siberian larch forest watersheds. Geochim. Cosmochim. Acta, 147: 76–89, doi:https://doi.org/10.1016/j.gca.2014.10.009https://doi.org/10.1016/j.gca.2014.10.009.
Moosdorf, N., Renforth, P., Hartmann, J., 2014. Carbon Dioxide Efficiency of Terrestrial Enhanced Weathering. Environmental Science & Technology, 48(9): 4809–4816, doi:https://doi.org/10.1021/es4052022https://doi.org/10.1021/es4052022.
Moynier, F., Fujii, T., 2017. Theoretical isotopic fractionation of magnesium between chlorophylls. Sci. Rep. 7 (1), 6973. https://doi.org/10.1038/s41598-017-07305-6.
Nai, C. et al., 2013. Nutritional physiology of a rock-inhabiting, model microcolonial fungus from an ancestral lineage of the Chaetothyriales (Ascomycetes). Fungal Genet. Biol., 56(0): 54–66, doi:https://doi.org/10.1016/j.fgb.2013.04.001 http://dx.doi.org/10.1016/j.fgb.2013.04.001.
Noack-Schönmann, S., et al., 2014. Genetic transformation of Knufia petricola A95—a model organism for biofilm-material interactions. AMB Express 4 (1), 80–85. https://doi.org/10.1186/s13568-014-0080-5.
Oelkers, E.H. et al., 2015. The efficient long-term inhibition of forsterite dissolution by common soil bacteria and fungi at Earth surface conditions. Geochim. Cosmochim. Acta, 168: 222–235, doi:https://doi.org/10.1016/j.gca.2015.06.004https://doi.org/10.1016/j.gca.2015.06.004.
Oelkers, E.H., Berninger, U.-N., Pérez-Fernàndez, A., Chmeleff, J., Mavromatis, V., 2018a. The temporal evolution of magnesium isotope fractionation during hydromagnesite dissolution, precipitation, and at equilibrium. Geochim. Cosmochim. Acta, 226: 36–49, doi:https://doi.org/10.1016/j.gca.2017.11.004https://doi.org/10.1016/j.gca.2017.11.004.
Oelkers, E.H., Declercq, J., Saldi, G.D., Gislason, S.R., Schott, J., 2018b. Olivine dissolution rates: a critical review. Chem. Geol., 500: 1–19, doi:https://doi.org/10.1016/j.chemgeo.2018.10.008https://doi.org/10.1016/j.chemgeo.2018.10.008.
Opfergelt, S. et al., 2014. Magnesium retention on the soil exchange complex controlling Mg isotope variations in soils, soil solutions and vegetation in volcanic soils, Iceland. Geochim. Cosmochim. Acta, 125: 110–130, doi:https://doi.org/10.1016/j.gca.2013.09.036https://doi.org/10.1016/j.gca.2013.09.036.
Parkhurst, D.L., Appelo, C.A.J., 1999. User's guide to PHREEQC (Version 2): a computer program for speciation, batch-reaction, one-dimensional transport, and inverse geochemical calculations. In: U.S. Geological Survey Water-Resources Investigations Report, pp. 99–4259. https://doi.org/10.3133/wri994259.
Pearce, C.R., Saldi, G.D., Schott, J., Oelkers, E.H., 2012. Isotopic fractionation during congruent dissolution, precipitation and at equilibrium: evidence from Mg isotopes. Geochim. Cosmochim. Acta, 92(0): 170–183, doi:https://doi.org/10.1016/j.gca.2012.05.045http://dx.doi.org/10.1016/j.gca.2012.05.045.
Pokharel, R. et al., 2017. Mg Isotope Fractionation during Uptake by a Rock-Inhabiting, Model Microcolonial Fungus Knufia petricola at Acidic and Neutral pH. Environmental Science & Technology, 51(17): 9691–9699, doi:10.1021/acs.est.7b01798https://doi.org/10.1021/acs.est.7b01798.
Pokharel, R. et al., 2018. Magnesium stable isotope fractionation on a cellular level explored by cyanobacteria and black fungi with implications for higher plants. Environmental Science & Technology, doi:https://doi.org/10.1021/acs.est.8b02238https://doi.org/10.1021/acs.est.8b02238.
Pokrovsky, O.S., Schott, J., 2000a. Forsterite surface composition in aqueous solutions: a combined potentiometric, electrokinetic, and spectroscopic approach. Geochim. Cosmochim. Acta, 64 (19): 3299–3312, doi:https://doi.org/10.1016/S0016-7037(00)00435-Xhttp://dx.doi.org/10.1016/S0016-7037(00)00435-X.
Pokrovsky, O.S., Schott, J., 2000b. Kinetics and mechanism of forsterite dissolution at 25 °C and pH from 1 to 12. Geochim. Cosmochim. Acta, 64(19): 3313–3325, doi:https://doi.org/10.1016/S0016-7037(00)00434-8http://dx.doi.org/10.1016/S0016-7037(00)00434-8.
Ra, K., Kitagawa, H., 2007. Magnesium isotope analysis of different chlorophyll forms in marine phytoplankton using multi-collector ICP-MS. J. Anal. At. Spectrom., 22(7): 817–821, doi:https://doi.org/10.1039/B701213Fhttps://doi.org/10.1039/B701213F.
Ra, K., Kitagawa, H., Shiraiwa, Y., 2010. Mg isotopes in chlorophyll-a and coccoliths of cultured coccolithophores (Emiliania huxleyi) by MC-ICP-MS. Mar. Chem., 122(1): 130–137, doi:https://doi.org/10.1016/j.marchem.2010.07.004https://doi.org/10.1016/j.marchem.2010.07.004.
Renforth, P., Pogge von Strandmann, P.A.E., Henderson, G.M., 2015. The dissolution of olivine added to soil: Implications for enhanced weathering. Appl. Geochem., 61: 109–118, doi:https://doi.org/10.1016/j.apgeochem.2015.05.016https://doi.org/10.1016/j.apgeochem.2015.05.016.
Rimstidt, J.D., Brantley, S.L., Olsen, A.A., 2012. Systematic review of forsterite dissolution rate data. Geochim. Cosmochim. Acta, 99: 159–178, doi:https://doi.org/10.1016/j.gca.2012.09.019https://doi.org/10.1016/j.gca.2012.09.019.
Rosling, A., Lindahl, B.D., Taylor, A.F.S., Finlay, R.D., 2004. Mycelial growth and substrate acidification of ectomycorrhizal fungi in response to different minerals. FEMS Microbiol. Ecol., 47(1): 31–37, doi:https://doi.org/10.1016/S0168-6496(03)00222-8 https://doi.org/10.1016/S0168-6496(03)00222-8.
Ryu, J.-S. et al., 2016. Experimental investigation of Mg isotope fractionation during mineral dissolution and clay formation. Chem. Geol., 445: 135–145, doi:https://doi.org/10.1016/j.chemgeo.2016.02.006https://doi.org/10.1016/j.chemgeo.2016.02.006.
Saldi, G.D., Daval, D., Morvan, G., Knauss, K.G., 2013. The role of Fe and redox conditions in olivine carbonation rates: an experimental study of the rate limiting reactions at 90 and 150°C in open and closed systems. Geochim. Cosmochim. Acta, 118: 157–183, doi:https://doi.org/10.1016/j.gca.2013.04.029https://doi.org/10.1016/j.gca.2013.04.029.
Schmitt, A.-D. et al., 2012. Processes controlling the stable isotope compositions of Li, B, Mg and ca in plants, soils and waters: a review. Compt. Rendus Geosci., 344 (11 − 12): 704–722, doi:https://doi.org/10.1016/j.crte.2012.10.002http://dx.doi.org/10.1016/j.crte.2012.10.002.
Schott, J., Berner, R.A., 1983. X-ray photoelectron studies of the mechanism of iron silicate dissolution during weathering. Geochim. Cosmochim. Acta, 47(12): 2233–2240, doi:https://doi.org/10.1016/0016-7037(83)90046-7https://doi.org/10.1016/0016-7037(83)90046-7.
Schott, J., Mavromatis, V., Fujii, T., Pearce, C.R., Oelkers, E.H., 2016. The control of carbonate mineral Mg isotope composition by aqueous speciation: Theoretical and experimental modeling. Chem. Geol., 445: 120–134, doi:https://doi.org/10.1016/j.chemgeo.2016.03.011http://dx.doi.org/10.1016/j.chemgeo.2016.03.011.
Schuessler, J.A., Kämpf, H., Koch, U., Alawi, M., 2016. Earthquake impact on iron isotope signatures recorded in mineral spring water. Journal of Geophysical Research: Solid Earth, 121(12): 8548–8568, doi:https://doi.org/10.1002/2016JB013408https://doi.org/10.1002/2016JB013408.
Schuiling, R.D., Krijgsman, P., 2006. Enhanced weathering: an effective and cheap tool to Sequester Co2. Clim. Chang., 74(1): 349–354, doi:https://doi.org/10.1007/s10584-005-3485-yhttps://doi.org/10.1007/s10584-005-3485-y.
Schuiling, R.D., Herk, J., Pietersen, H.S., 1986. A potential process for the neutralisation of industrial waste acids by reaction with olivine. Geologie & Mijnbouw 65 (3), 243–246.
Seiffert, F., Bandow, N., Kalbe, U., Milke, R., Gorbushina, A.A., 2016. Laboratory tools to quantify biogenic dissolution of rocks and minerals: a model rock biofilm growing in percolation columns. Front. Earth Sci., 4(31), doi:https://doi.org/10.3389/feart.2016.00031 https://doi.org/10.3389/feart.2016.00031.
Shirokova, L.S. et al., 2013. Using Mg isotopes to trace cyanobacterially mediated magnesium carbonate precipitation in alkaline lakes. Aquat. Geochem., 19(1): 1–24, doi:https://doi.org/10.1007/s10498-012-9174-3https://doi.org/10.1007/s10498-012-9174-3.
Sissmann, O. et al., 2013. The deleterious effect of secondary phases on olivine carbonation yield: Insight from time-resolved aqueous-fluid sampling and FIB-TEM characterization. Chem. Geol., 357: 186–202, doi:https://doi.org/10.1016/j.chemgeo.2013.08.031https://doi.org/10.1016/j.chemgeo.2013.08.031.
Taylor, L.L. et al., 2015. Enhanced weathering strategies for stabilizing climate and averting ocean acidification. Nat. Clim. Chang., 6: 402, doi:https://doi.org/10.1038/nclimate2882https://doi.org/10.1038/nclimate2882.
Tipper, E.T., Gaillardet, J., Louvat, P., Capmas, F., White, A.F., 2010. Mg isotope constraints on soil pore-fluid chemistry: evidence from Santa Cruz, California. Geochim. Cosmochim. Acta, 74(14): 3883–3896, doi:https://doi.org/10.1016/j.gca.2010.04.021http://dx.doi.org/10.1016/j.gca.2010.04.021.
Torres, M.A., West, A.J., Nealson, K., 2014. Microbial acceleration of olivine dissolution via siderophore production. Procedia Earth and Planetary Science, 10: 118–122, doi:https://doi.org/10.1016/j.proeps.2014.08.041https://doi.org/10.1016/j.proeps.2014.08.041.
Uhlig, D., Schuessler, J.A., Bouchez, J., Dixon, J.L., von Blanckenburg, F., 2017. Quantifying nutrient uptake as driver of rock weathering in forest ecosystems by magnesium stable isotopes. Biogeosciences, 14(12): 3111–3128, doi:10.5194/bg-14-3111-2017https://doi.org/10.5194/bg-14-3111-2017.
Warcup, J.H., 1951. The ecology of soil fungi. Trans. Br. Mycol. Soc., 34(3): 376–399, doi:https://doi.org/10.1016/S0007-1536(51)80065-2https://doi.org/10.1016/S0007-1536(51)80065-2.
White, A.F., Brantley, S.L., 2003. The effect of time on the weathering of silicate minerals: why do weathering rates differ in the laboratory and field? Chem. Geol., 202(3–4): 479–506, doi:https://doi.org/10.1016/j.chemgeo.2003.03.001http://dx.doi.org/10.1016/j.chemgeo.2003.03.001.
Wiederhold, J.G. et al., 2006. Iron isotope fractionation during proton-promoted, ligand-controlled, and reductive dissolution of goethite. Environmental Science & Technology, 40(12): 3787–3793, doi:https://doi.org/10.1021/es052228yhttp://dx.doi.org/10.1021/es052228y.
Wimpenny, J. et al., 2010. The behaviour of Li and Mg isotopes during primary phase

dissolution and secondary mineral formation in basalt. Geochim. Cosmochim. Acta, 74(18): 5259–5279, doi:https://doi.org/10.1016/j.gca.2010.06.028http://dx.doi.org/10.1016/j.gca.2010.06.028.

Wimpenny, J., Colla, C.A., Yin, Q.-Z., Rustad, J.R., Casey, W.H., 2014. Investigating the behaviour of Mg isotopes during the formation of clay minerals. Geochim. Cosmochim. Acta, 128: 178–194, doi:https://doi.org/10.1016/j.gca.2013.12.012https://doi.org/10.1016/j.gca.2013.12.012.

Wogelius, R.A., Walther, J.V., 1991. Olivine dissolution at 25°C: Effects of pH, CO2, and organic acids. Geochim. Cosmochim. Acta, 55(4): 943–954, doi:https://doi.org/10.1016/0016-7037(91)90153-Vhttp://dx.doi.org/10.1016/0016-7037(91)90153-V.

Wollenzien, U., de Hoog, G.S., Krumbein, W., Uijthof, J.M.J., 1997. Sarcinomyces petricola, a new microcolonial fungus from marble in the Mediterranean basin. Antonie Van Leeuwenhoek, 71(3): 281–288, doi:https://doi.org/10.1023/a:1000157803954http://dx.doi.org/10.1023/a:1000157803954.

Young, E.D., Galy, A., 2004. The isotope geochemistry and cosmochemistry of magnesium. Rev. Mineral. Geochem., 55(1): 197–230, doi:https://doi.org/10.2138/gsrmg.55.1.197http://dx.doi.org/10.2138/gsrmg.55.1.197.

Ziegler, K., Chadwick, O.A., Brzezinski, M.A., Kelly, E.F., 2005. Natural variations of δ30Si ratios during progressive basalt weathering, Hawaiian Islands. Geochim. Cosmochim. Acta 69 (19), 4597–4610. https://doi.org/10.1016/j.gca.2005.05.008.